micromachines

MDPI

Article

Mathematical Modelling and Simulation Research of Thermal Engraving Technology Based on PMMA Material

Xiaowei Han *, Xiaowei Liu † and Li Tian †

Key Laboratory of Micro-systems and Micro-structures Manufacturing, Harbin Institute of Technology, Harbin 150000, China; lxw@hit.edu.cn (X.L.); tianli@hit.edu.cn (L.T.)

* Correspondence: hanxw2016@outlook.com; Tel.: +86-139-4508-4159

† These authors contributed equally to this work.

Academic Editor: Jeong-Bong Lee

Received: 30 November 2015; Accepted: 22 February 2016; Published: 26 February 2016

Abstract: We proposed a thermal engraving technology based on heat transfer theory and polymer rheology in microfluidic field. Then, we established a 3D model of the thermal engraving process based on polymethyl methacrylate (PMMA) material. We could employ the model to analyze the influence of temperature and speed on microchannel processing through the finite element simulation. Thus, we gained the optimal processing parameters. The orthogonal experiments were carried out within the parameter ranges obtained by the simulation results. Finally, we fabricated the smooth microchannel, the average roughness of which was 0.3 μm, by using the optimal parameters. Furthermore, we examined the surface morphology and wettability. Our work provides a convenient technological support for a fast, low-cost, and large-scale manufacturing method of microfluidic chips.

Keywords: microchannel; MEMS; microfluidic chip

1. Introduction

There were many detection modes in trace detection in microfluidic field, such as photoelectric detection and capacitance coupled contactless conductivity detection in K^+ testing [1,2]. With the development of this technology, many researchers conducted studies on the microfabrication technologies of rigid polymers. Polymer microfluidic chips were fabricated by means of silicon dry etching, electroplating and injection molding. The method could be used for fabrication of microchannels. The depth of microchannels were in the range between 100 nm and 100 μm [3]. However, this fabrication process needed direct photolithography method. Besides, microstructures could be fabricated by using hot embossing techniques in polymethyl methacrylate (PMMA) from Ni-based molding dies in 5 min. The dies were prepared by using LIGA (Lithographie, Galvanoformung, Abformung) technology [4]. The PMMA microfluidic chip could also be fabricated by means of copper master hot embossing. However, the copper master used the electroplating mold technology for forming the microstructures [5]. We found that the hot embossing method should involve indirect photolithography technology, or even combine several fabrication processes at the same time. Those methods significantly increased preparation time, cost, and complexity. The microchannel should also be processed without photolithography technologies, such as laser ablation method. The PMMA microchannels were fabricated by CO_2 laser processing method. The two-pass laser was used to fabricate microchannel. Then, the width of microchannel was usually on the level of one hundred micrometer [6,7]. However, the size of PMMA microchannels were big when the CO_2 laser was involved. The Nd: YAG solid-state laser was used to fabricate smaller

size microchannels. The minimum average width of microchannel was 97 μm, and the minimum average depth was 36 μm [8]. Furthermore, the microchannels were fabricated by femtosecond laser technology [9]. The average surface roughness of PMMA microchannel was only 0.3 μm when the femtosecond laser was involved [10,11]. However, the femtosecond laser is usually expensive. This article proposes a thermal engraving technique applied to PMMA material and establishes the corresponding simulation models. This technique can be applied for the fabrication of microchannels in microfluidic chips without the need for photolithography. In view of the large differences of rheological mechanism between thermal engraving process and other microchannel processing methods, the modeling methods of other microchannel processing techniques are not applicable to rheological mechanism analysis of thermal engraving process. In this study, based on the rheological mechanism analysis of the thermal engraving process, a model was established. According to simulation results, reasonable experimental parameter ranges were determined, to provide technical basis for experimental studies of thermal engraving.

2. Design of Experimental System

We designed and manufactured the thermal engraving system which was used to carry out the experiments. The thermal engraving system is composed of control system and mechanical system. The control system includes a temperature controller, a step motor, and an upper computer. The temperature controller and the step motor controller are used for the precise control of temperature and movement of the objective table. The mechanical system includes mainly a rack, a thermal engraving depth controller, a heater, a step motor, a microgravier, and a two-degrees-of-freedom (2-DOFs) objective table. By using the thermal engraving depth controller, the thermal engraving depth of microchannels is set. The step motor accurately controls the movement velocity of the objective table and the heater heats the microgravier. The block diagram of the thermal engraving system is shown in Figure 1.

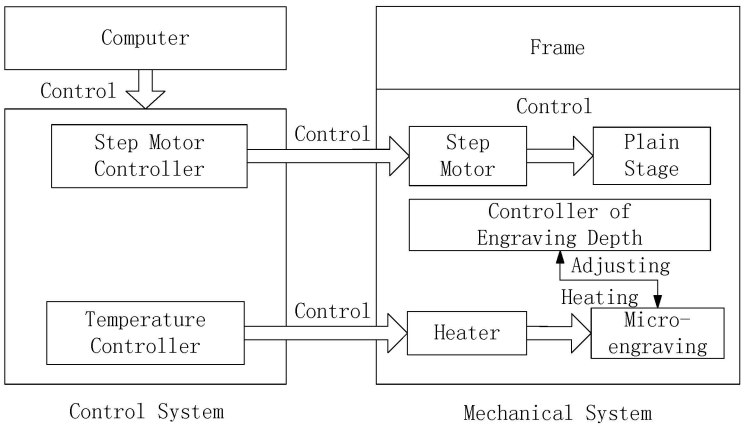

Figure 1. The block diagram of thermal engraving system design.

The temperature controller is composed of a PID (Proportion, Integration, Differentiation) controller and a K-type thermocouple. The thermocouple could convert the temperature changes to current changes and feedbacks to the PID controller. We use self-tuning function to control the temperature of microgravier during the experiment [12]. The step motor controller circuit consists of a power circuit, a step motor drive circuit and a universal serial bus (USB) drive circuit. During the thermal engraving process, the step motor controller transforms the control signal into the step motor angular displacement. Since the step motor rotates a fixed angle in each pulse single, its angular displacement can be controlled by adjusting the number of pulses. Furthermore, by varying the frequency, both the step motor rotary speed and acceleration can be adjusted. Finally, the movements of the objective table can be precisely controlled.

Figure 2 illustrates the thermal engraving process. The PMMA substrate was fixed on the objective table. The rotary speed of step motor was set through the computer software interface. Then, we set the PID controller to self-tuning mode. The temperature of the microgravier would reach the setting value after the self-tuning process. Therefore, we can carry out the thermal engraving experiments.

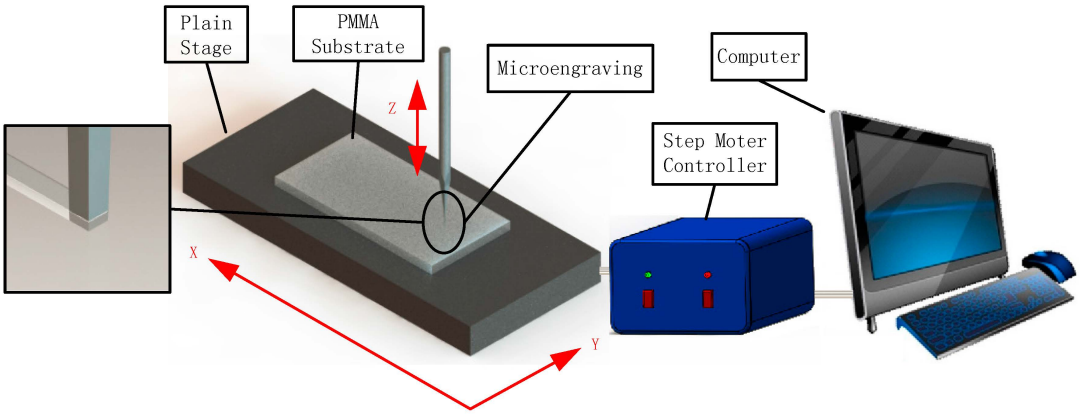

Figure 2. The schematic of thermal engraving process.

3. Modeling, Simulation and Result Analysis

Using the established microgravier heat transfer model, the temperature gradient of the microgravier at different temperatures was simulated. The simulation results can provide the theoretical basis for analyzing the heat transfer characteristics of the microgravier and PMMA material. Moreover, based on the simulation results the PMMA viscous flow range around the microgravier can be determined, and the geometric model of PMMA viscous flow built. By analyzing the forces applied on the PMMA viscous flow under the conditions with varying technological parameters, a reasonable range for technological parameters in thermal engraving experiments can be concluded.

3.1. Thermal Micorgravier Head Heat Transfer Analysis

Since the temperature controller maintains the microgravier at a preset temperature, we mainly focused on the steady-state heat transfer model of the microgravier. One assumes that during the modeling process the heater heat completely transfers to the microgravier. The contact area between the microgravier and the air far exceeds the contact area between the microgravier and the PMMA material; therefore, only the thermal transfer between microgravier and air was modeled, neglecting the effects induced by heat transfer between microgravier and PMMA material. Finally, when simulating the microgravier temperature distribution, the air temperature was set to room temperature.

3.1.1. Geometric Model

Figure 3 displays the geometric model and the photo of a rectangular microgravier. Figure 3b is a photo of the minimum rectangular microgravier which we could fabricate. To reduce the computational load, only the connecting part between microgravier and heater has been modeled. Therefore, the temperature at the cross section of microgravier is the heater heating temperature.

The microgravier main body is a tungsten steel bar whose diameter is 3.75 mm. The characteristic size (width) of the microgravier head is 100 μm; thus, a large geometric size span exists. Therefore, a reasonable finite element mesh generation of the geometrical model improves the simulation precision.

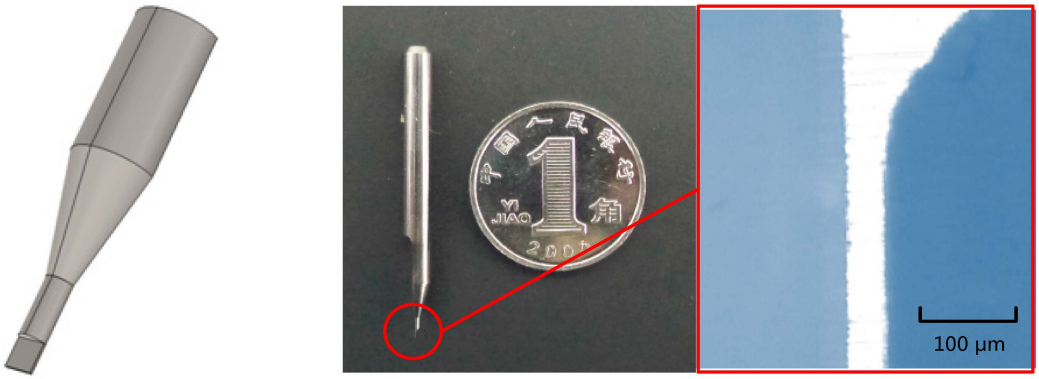

(**a**) (**b**)

Figure 3. The geometric model and the photo of a rectangular engraving microgravier: (**a**) The geometric model of a rectangular engraving microgravier; (**b**) The photo of a rectangular engraving microgravier.

3.1.2. Microgravier Head Heat Transfer Analysis

Figure 4 displays the surface temperature distribution of thermal microgravier. When the temperature of the heating zone is 120 °C, the microgravier head temperature is only 90 °C, *i.e.*, with a temperature difference of 30 °C. As shown in the partial enlarged view of the surface temperature distribution of the microgravier head, the geometrical size decreases rapidly while the ratio of surface to volume increases. However, since the microgravier head length is only 2 mm, its temperature gradient exhibits no obvious increase.

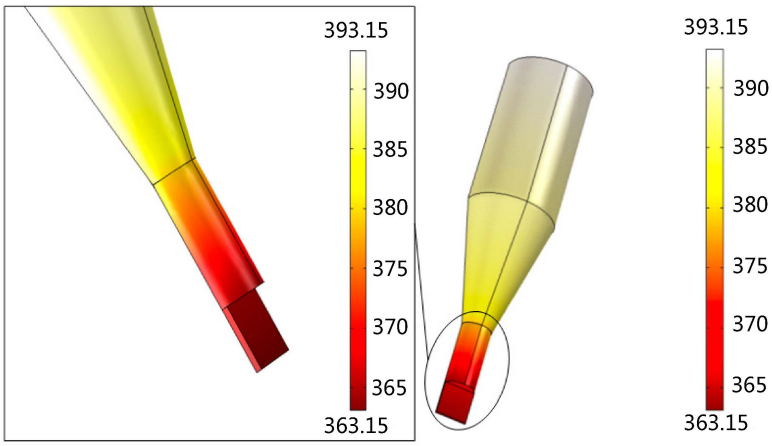

Figure 4. The surface temperature distribution of the thermal engraving microgravier.

Several cross sections were selected along the axial direction of thermal microgravier for further analyzing its heat transfer behavior. As Figure 5 shows, when the temperature of the heating zone is 120 °C the temperature gradient in the microgravier head is less than 3 °C. Due the difference between the size of the microgravier head length and the depth of thermal engraving, the temperature gradient of the contact area between the micro-engraver and PMMA can be neglected.

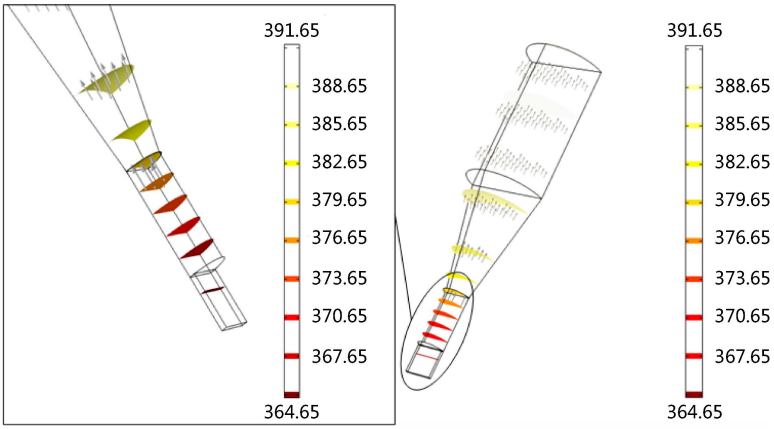

Figure 5. The cross sectional view of temperature distribution of the thermal engraving microgravier.

3.2. Temperature Distribution of PMMA Materials

During thermal engraving process, when the temperature parameter is fixed, the thermal engraving velocity can influence the material temperature distribution. Figure 6 shows the temperature distributions of PMMA materials when the temperature parameter is 91 °C, and the thermal engraving velocities are 1 mm/s, 2 mm/s, 3 mm/s and 4 mm/s, respectively. The viscous transition temperature of PMMA materials was 89 °C. At 91 °C, the viscous flow range of PMMA near the microgravier head is quite small; at temperatures less than 89 °C, PMMA materials around the microgravier head become non-viscous flow. When the applied force exceeds the elastic limit, fractures may occur in non-viscous PMMA materials, thus it is difficult to fabricate microchannels with smooth surface morphology. Therefore, the thermal engraving velocity should be matched with heat transfer velocity, to keep PMMA near the microgravier always in the viscous flow state. Moreover, as the thermal engraving velocity increases, the isothermal surface of PMMA near the engraver head shrinks gradually towards the microgravier head.

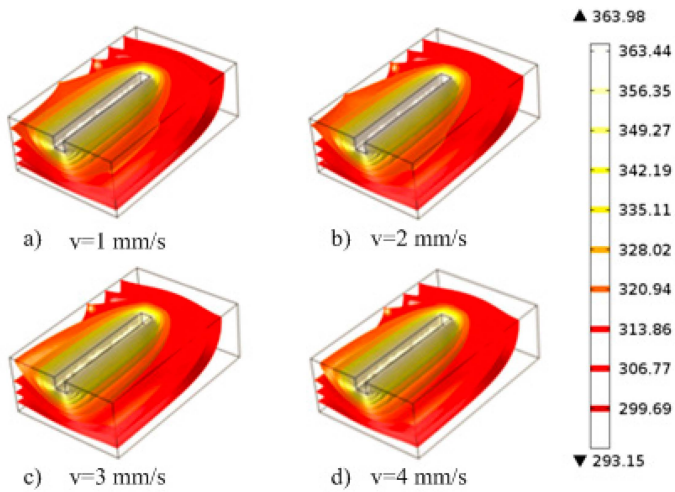

Figure 6. The cross-sectional view of temperature distribution at different thermal engraving speed: (**a**) v = 1 mm/s; (**b**) v = 2 mm/s. (**c**) v = 3 mm/s; (**d**) v = 4 mm/s.

When the thermal engraving velocity increases to a certain degree, the microgravier head velocity will exceed the heat transfer velocity, *i.e.*, the thermal engraving velocity may not match the temperature. At this moment, there will exists insufficient PMMA viscous flow layer along the movement direction of microgravier head, and the microgravier head will directly contact the

elastomeric-state or glassy-state PMMA materials. Figure 7 shows the temperature distribution of PMMA material when the temperature is 91 °C and the thermal engraving velocity is 5 mm/s. PMMA materials within the range of 10 μm around the microgravier head are all in non-viscous flow state when the temperature is 96 °C. Consequently, at 91 °C, the thermal engraving velocity should not exceed the upper limit of 5 mm/s. When the velocity exceeds this limit, it became hard to fabricate micro-channels with smooth surface topography. When the temperature increases, since the temperature gradients of the microgravier head and PMMA increase, a higher upper limit of thermal engraving velocity is allowed.

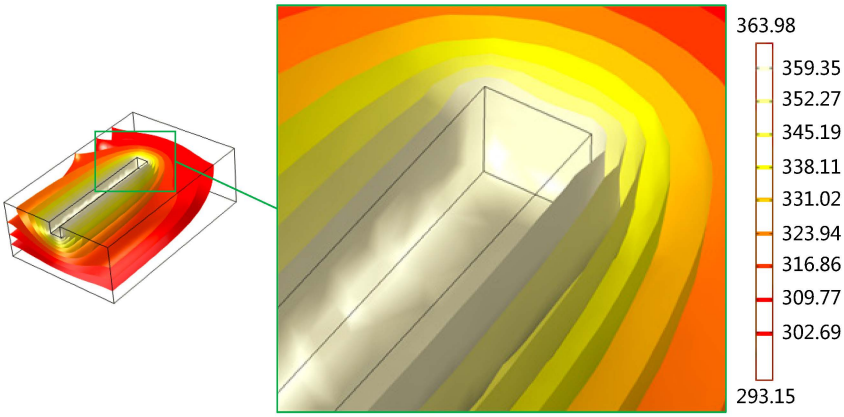

Figure 7. The cross-sectional view of temperature distribution when the thermal engraving speed is higher than the heat transfer rate.

3.3. Thermal Engraving Model

During the modeling of the heat transfer between microgravier head and PMMA viscous flow, the material specific heat capacity and thermal conductivity are relatively low and the viscous flow steadily extrudes. The heat exchange between the extruded PMMA viscous flow and air during the dynamical thermal engraving process is thus neglected. Since the temperature controller keeps the microgravier head temperature at a constant value, the heat exchange with PMMA material does not reduce the surface temperature of microgravier head. Moreover, when simulating the heat transfer model between microgravier head and PMMA material the initial temperature of PMMA was set to room temperature (20 °C).

3.3.1. Construction of the Geometric Model of the Viscous Flow Microchannels

Figure 8 shows the microchannel geometrical model during thermal engraving process when a rectangular thermal microgravier with both depth and width of 100 μm was used. To highlight viscous flow movements into substrate, the microgravier head was modeled transparent; the outside surface of the head was set as the internal geometric boundary. Besides, the extruded viscous flow is irrelevant in micro-channel processing and therefore the front viscous flow of PMMA has not been modeled.

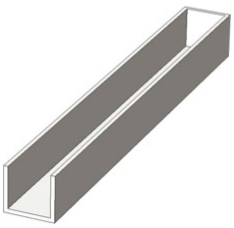

Figure 8. The geometrical model a 100 μm width rectangular microchannel in the thermal engraving process.

3.3.2. Temperature Field Distribution in the Viscous Flow Channel

Figure 9a displays the temperature distribution of the PMMA viscous flow during the thermal engraving process when the microgravier head temperature is 96 °C and the velocity is 3.2 mm/s. Since the PMMA viscous flow was constantly extruded along the microgravier head movement direction, the temperature of the microgravier head is obviously lower than that of the PMMA viscous flow on its both sides. Figure 9b shows the isothermal profile of the PMMA viscous flow during the engraving process. The distance between two isothermal surfaces of PMMA viscous flow below the microgravier head is relatively large. This means that the temperature gradient of the viscous flow on the bottom of the head decreases gradually along the vertical direction because the heat conductivity coefficient and specific heat capacity of PMMA viscous flow are small, and thereby the heat transfer inside the viscous flow is quite slow. Besides, since the microgravier is in motion, the head-on heat flux along the microgravier movement direction is larger. This leads to a greater temperature gradient of PMMA viscous flow in front of the microgravier head while the temperature gradient along the normal direction of the microgravier movement is smaller. Meanwhile, the temperature in front of the microgravier is much lower than those on two sides and on bottom of the microgravier head.

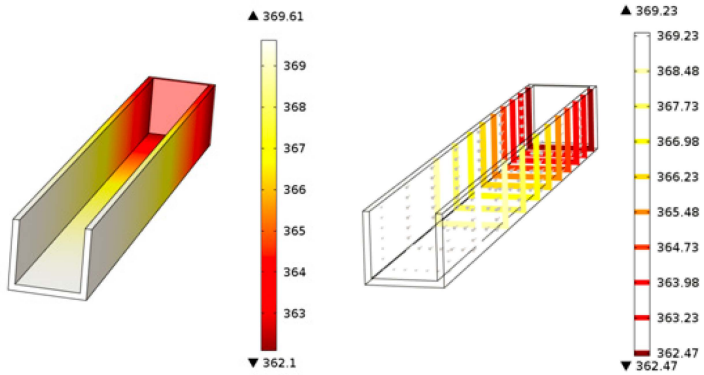

(**a**) (**b**)

Figure 9. The temperature of the polymethyl methacrylate (PMMA) viscous flow: (**a**) The temperature distribution of the PMMA viscous flow; (**b**) The isothermal sectional view of PMMA viscous flow.

3.3.3. Viscous Flow Field Distribution

Figure 10 shows the flow field distribution of the PMMA viscous flow around the microgravier head during thermal engraving process. The flow velocity of the PMMA viscous flow around the microgravier is relatively large. As the thickness of viscous flow increases, the flow velocity near the boundary of viscous flow microchannel decreases gradually.

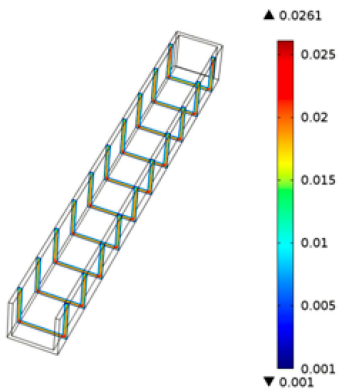

Figure 10. The flow field of the PMMA viscous flow.

3.3.4. Viscous Flow Pressure Distribution

Under the effect of thermal microgravers movements, the head-on PMMA viscous flow in the microgravers head movement direction would be squeezed by microgravers head. Figure 11 shows the pressure distribution profile of the PMMA viscous flow: the pressure on the head-on viscous flow in the microgravers head movement direction is the largest and decreases gradually along the microchannel (in a backwards direction).

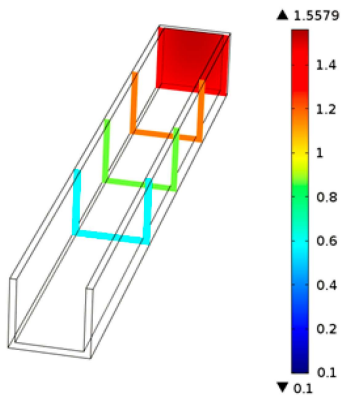

Figure 11. The cross-sectional view of the pressure distribution of the PMMA viscous flow.

3.3.5. Viscous Flow Microchannel Pressure Distribution

The PMMA viscous flow stress analysis gives its pressure distribution. According to Figure 12, when the PMMA viscous flow extrudes from the front of microgravers head, the pressure on the head-on viscous flow in the microgravers head movement direction is the largest and decreases gradually backwards. Since some viscous flow extrudes from the top, the pressure at the exit of the viscous flow decreases slightly.

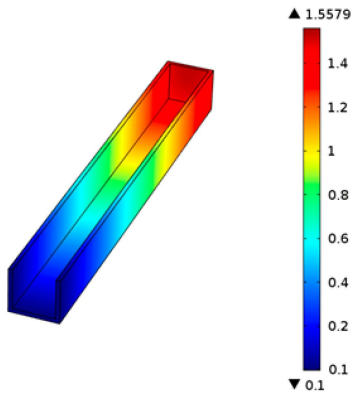

Figure 12. The pressure distribution of the PMMA viscous flow.

3.4. Result Analysis

The thermal engraving model presents the 3D results of temperature distribution, flow distribution, viscous field stress distribution, and boundary pressure distribution of PMMA viscous flow under specific technological parameters. However, the simulation analyses using a single group of technological parameters can hardly offer a clear and regular understanding of the thermal engraving process or determine a reasonable technological parameters range. Therefore, the simulation results of the PMMA viscous flow under different parameters have been systematically analyzed, to obtain the trend of simulation results.

3.4.1. Effects of the Temperature

With the same thermal engraving velocity, different temperatures would impose a certain effect on the viscosity of the flow and then affect the pressure distribution of the viscous flow. When the stress was applied on the viscous flow through the microgravier head, the generated pressure affected the microchannel fabrication. Figure 13 shows the variation of pressure on the viscous flow with temperature along the normal direction of the microgravier head movements.

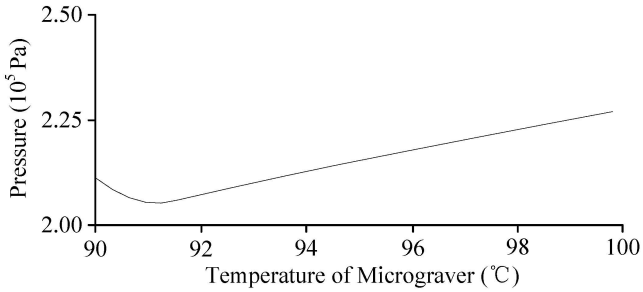

Figure 13. The relationship between temperature and pressure of viscous flow on the normal movement direction of microgravier.

3.4.2. Effects of the Speed

Changes in velocity can lead to the variation of pressure on the PMMA viscous flow around the microgravier head. Figure 14 shows the pressure on the PMMA viscous flow when the microgravier head velocity exhibits a normal spatial relation with its movement direction.

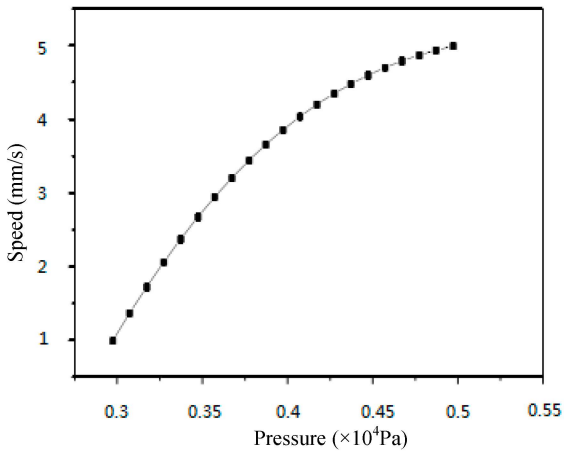

Figure 14. The relationship between the speed and the pressure of viscous flow on the normal direction of microgravier.

4. Microchannel Characterization

4.1. Surface Topography Characterization

Orthogonal tests were performed using the parameters determined by numerical simulations, and finally the optimal technological parameters were acquired. When the thermal engraving velocity is 4.2 mm/s and the temperature is 91 °C, the 0.3 μm rough microchannels can be fabricated by thermal engraving depth ranging from 30 to 200 μm. The thickness deviation of PMMA plant we involved was between 10 and 20 μm. So, we couldn't guarantee the fabrication quality if the thermal engraving depth was below 30 μm. Figure 15a illustrates a cross-sectional image of rectangular microchannel. Figure 15b shows the atomic force microscope (AFM) image of microchannel bottom surface.

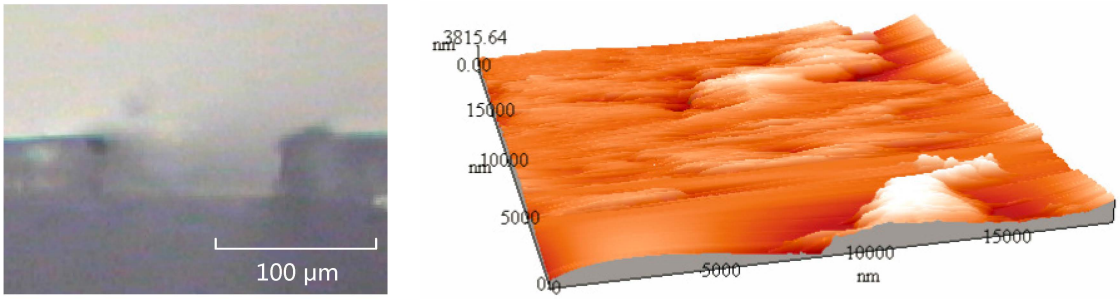

(**a**) (**b**)

Figure 15. The features of rectangular microchannel: (**a**) The cross-sectional image of rectangular microchannel; (**b**) The atomic force microscope (AFM) image of microchannel.

Figure 16 shows a 30 μm width rectangular micro-channel; its size can be comparable to the size of microchannels fabricated by means of lithography or laser techniques [13,14].

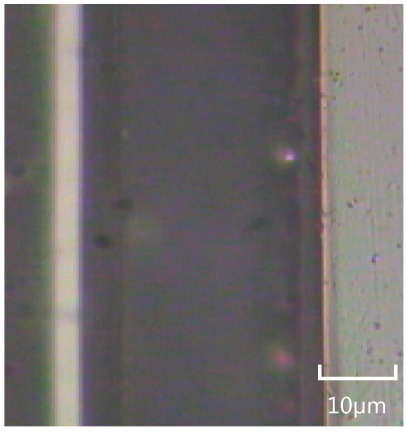

Figure 16. The 30 μm width rectangular microchannel.

We supply the comparison as Table 1. In this table, we compare our method with some representative methods, such as laser ablation method, hot embossing method and so on.

Table 1. The comparison of microchannel fabricating methods based on PMMA.

Method	Microchannel Size (μm)	Surface Roughness (μm)	Process Cycle (min)	Assistant Technology	Cost	Literature
Injection moulding	48 × 110	<0.001	-	EDM, PVD	High	[15]
CO_2 laser ablation	150 × 50	25	<1	None	Low	[7]
Femtosecond laser ablation	100 × 20	0.05–0.3	<1	Chloroform vapor Treatment	Low	[11]
PCB mold hot embossing	400 × 25	0.56 ± 0.13	5	UV Lithography	Low	[16]
SU-8 mold hot embossing	15 × 50	0.7	60–80	UV Lithography	High	[17]
Thermal engraving	30 × 30	0.3	<1	None	Lower	This paper

We find the thermal engraving method gain some advantages microchannel size, process cycle and cost. Moreover, this method don't involve any assistant technology, such as electrical discharge machining (EDM), physical vapor deposition (PVD) and ultraviolet lithography (UV Lithography).

4.2. Wettability Characterization

During thermal engraving, temperature and velocity may affect the microchannel wettability to a certain degree. The wettability can then affect the flow resistance of the solution in the microchannel. Therefore, in the present work heating temperature of the microgravier head and microchannel surface roughness characterize microchannel wettability.

4.2.1. Effects of Temperature on Microchannel Surface Wettability

Surface free energy γ_{sv} (*i.e.*, surface tension) and surface roughness are two primary factors usually affecting wettability. However, for solid materials, γ_{sv} measurement is a difficult task. Thus, we use the contact angle between liquid and PMMA surface to assess the variation of the solid surface energy. Therefore, we designed a set of experiments to assess the effects of the thermal engraving temperature on the surface energy of PMMA material. So, we could studied the effects of thermal engraving temperature on micro-channel wettability.

The PMMA substrate was only heated by vacuum drying oven without any engraving and the variation of contact angle directly reflects the effect of temperature variation on wettability of PMMA materials. The substrate was heated within the range 89 °C to 95 °C. Experimental data are show in Table 2. The larger contact angle means poorer hydrophilicity. We found the hydrophilic decreased with the increase of temperature. The experimental data also show the change of water contact angle is 4.8% in the temperature range of 89–90 °C. So, we could deduce the effects of temperature parameter on the hydrophilicity is limited.

Table 2. The relationship between heating temperature and contact angle.

Temperature (°C)	89	90	91	92	93	94	95
Contact angle (°)	77.4	77.8	78.3	79.4	79.9	80.6	81.1

4.2.2. Effects of Roughness on Microchannel Surface Wettability

At the gas-liquid interface, the microchannel wettability can be evaluated by observing the flow pattern in front of the liquid. The liquid flowing head, convex or concave, would indeed be influenced by the pressure of the flowing. We did not bond the microchannel in the process of hydrophilic test. Thus, we couldn't apply any pressure since we considered the pressure's influence. It is a kind of natural flowing without any external force applied to the liquid flowing. Figure 17a shows a flat and smooth microchannel using the optimal technological parameters. At the gas-liquid interface the meniscus can be observed, *i.e.*, the microchannel is hydrophilic. By way of comparison, Figure 17b shows a rough microchannel using non-ideal technological parameters. There is so meniscus at the gas-liquid interface, *i.e.*, the microchannel is hydrophobic.

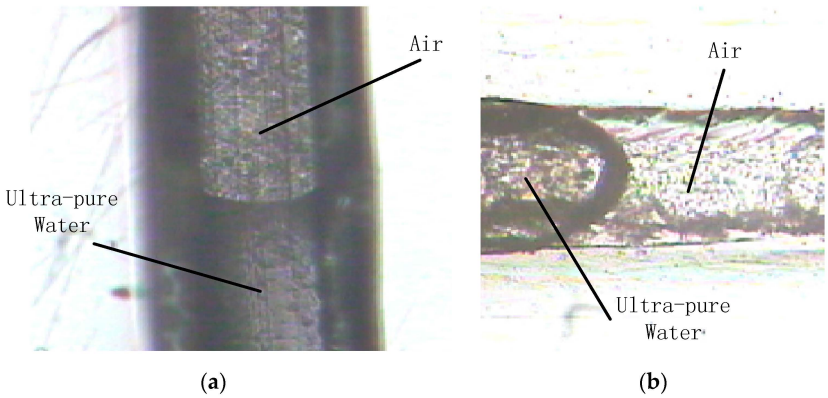

Figure 17. The wettability of microchannels: (**a**) Hydrophilic microchannel; (**b**) Hydrophobic microchannel.

5. Conclusions

In this paper, a thermal engraving microchannel fabrication technique without the application of lithography was proposed and the related manufacturing process model was constructed. In the model, the stresses on the viscous flow around the micrograver head using different technological parameters were analyzed and the reasonable range of technological parameters was then determined. Results show that, when the temperature ranges from 90 to 95 °C, the stress on the viscous flow around the micrograver head is relatively small. Moreover, as the velocity increases, the pressure on the normal direction of the micrograver movements increases nonlinear. Finally, orthogonal experiments were conducted using the selected optimal technological parameters, and a microchannel with the roughness and minimum characteristic sizes of 0.3 and 30 μm, respectively was fabricated. The experimental results indicate that when the microchannel was fabricated under the condition with optimal technological parameters has flat and smooth surface, and thus is hydrophilic; on the contrary, under non-ideal parameters is characterized by rough surface and hydrophobicity. The presented results are applicable to the analytical chemistry laboratory with no superclean room and expensive lithography equipment, which can also be further extended to the micro-channels fabrication in non-crystalline and linear polymers applicable to microfluidic fields.

Acknowledgments: Research of epithelial cell differentiation and its electrophy-siological index monitoring based on LOC key techniques.

Author Contributions: Xiaowei Han and Xiaowei Liu conceived and designed the experiments; Xiaowei Han performed the experiments; Xiaowei Han and Li Tian established the model and analyzed the data; Xiaowei Liu contributed reagents/materials/analysis tools; Xiaowei Han wrote the paper.

Conflicts of Interest: The authors declare no conflict of interest.

References

1. Ren, M.Y.; Tian, L. Design and simulation of photoelectric detection circuit for microfluidics chip. *Appl. Mech. Mater* **2013**, *384*, 3308–3311. [CrossRef]
2. Xu, Y.; Liang, J. Characterization of a capacitance coupled contactless conductivity detection system with sidewall electrodes on a low voltage driven electrophoresis microchip. *Anal. Bioanal. Chem.* **2010**, *397*, 1583–1593. [CrossRef] [PubMed]
3. Matteucci, M.; Christiansen, T.L. Fabrication and characterization of injection molded multi level nano and microfluidic systems. *Microelectron. Eng.* **2013**, *111*, 294–298. [CrossRef]
4. Qi, S.; Liu, X. Microfluidic devices fabricated in poly (methylmethacrylate) using hot-embossing with integrated sampling capillary and fiber optics for fluorescence detection. *Lab Chip* **2002**, *2*, 88–95. [CrossRef] [PubMed]
5. Nugen, S.R.; Asiello, P.J. Design and fabrication of a microfluidic device for near-single cell mRNA isolation using a copper hot embossing master. *Microsyst. Technol.* **2009**, *15*, 477–483. [CrossRef]
6. Prakash, S.; Kumar, S. Profile and depth prediction in single pass and two pass CO_2 laser microchanneling process. *J. Micromech. Microeng.* **2015**, *25*, 035010. [CrossRef]
7. Romoli, L.; Tantussi, G.; Dini, G. Experimental approach to the laser machining of PMMA substrates for the fabrication of microfluidic devices. *Opt. Lasers Eng.* **2011**, *49*, 419–427. [CrossRef]
8. Criales, L.E.; Orozco, P.F. Effect of fluence and pulse overlapping on fabrication of microchannels in PMMA/PDMS via UV laser micromachining: modeling and experimentation. *Mater. Manuf. Processes* **2015**, *30*, 890–901. [CrossRef]
9. Chang, T.L. Micromachining of microfluidic channels in glass by microjoule femtosecond laser pulses. *Microelectron. Eng.* **2013**, *110*, 450–456. [CrossRef]
10. De, M.C.; Eaton, S.M. Solvent vapor treatment controls surface wettability in PMMA femtosecond laser ablated microchannels. *Microfluid Nanofluid* **2013**, *14*, 171–176.
11. Chung, C.K.; Lin, S.L. On the fabrication of minimizing bulges and reducing the feature dimensions of microchannels using novel CO_2 laser micromachining. *J. Micromech. Microeng.* **2011**, *21*, 1–7.

12. Tao, Y.H. *The New PID Control and Its Application*, 1st ed.; Machinery Industry Press: Beijing, China, 1998; pp. 27–35.
13. Kobayashi, H.; Takahashi, H. Viscosity measurement of organic glasses below and above glass transition temperature. *J. Non-Crystal. Solids* **2001**, *290*, 32–40. [CrossRef]
14. Wang, L.; Li, Q. Scale effect on filling stage in micro-injection molding for thin slit cavities. *Microsyst. Technol.* **2012**, *18*, 2085–2091. [CrossRef]
15. Tosello, G.; Marinello, F.; Hansen, H.N. Characterisation and analysis of microchannels and submicrometre surface roughness of injection moulded microfluidic systems using optical metrology. *Plast. Rubber Compos.* **2012**, *41*, 29–39. [CrossRef]
16. Jiang, J.; Zhan, J.; Yue, W. A single low-cost microfabrication approach for polymethylmethacrylate, polystyrene, polycarbonate and polysulfone based microdevices. *RSC Adv.* **2015**, *5*, 36036–36043. [CrossRef]
17. Shamsi, A.; Amiri, A.; Heydari, P. Low cost method for hot embossing of microstructures on PMMA by SU-8 masters. *Microsyst. Technol.* **2014**, *20*, 1925–1931. [CrossRef]

© 2016 by the authors; licensee MDPI, Basel, Switzerland. This article is an open access article distributed under the terms and conditions of the Creative Commons by Attribution (CC-BY) license (http://creativecommons.org/licenses/by/4.0/).